This article has been accepted for publication in a future issue of this journal, but has not been fully edited. Content may change prior to final publication. Citation information: DOI 10.1109/TIM.2021.3139688, IEEE Transactions on Instrumentation and Measurement

A Signal Segmentation Approach to Identify Incident/Reflected Traveling-Waves for Fault Location in Half-Bridge MMC-HVDC Grids

Mohammad Farshad, and Mazaher Karimi, *Member, IEEE*

***Abstract*--This article presents a new systematic technique for identifying voltage traveling-waves (TWs) to determine the location of line faults in half-bridge modular multilevel converter-based high-voltage direct-current (HBMMC-HVDC) grids. In this technique, the buffered voltage signal frame around the fault-detection time is first scaled and then segmented via an optimization process. Finally, the incident/reflected TWs arrival times are obtained by executing a simple search algorithm on the reconstructed signal segments' differences. This article describes how to use this technique in three forms of TW-based fault location schemes, including the single-ended scheme with known TW velocity, the double-ended scheme with known TW velocity, and the double-ended scheme with unknown TW velocity. The application results on a 4-terminal HBMMC-HVDC grid simulated with exact component models show the proposed technique's high capability and accuracy in all the three TW-based fault-location schemes. According to these results, the average fault-location errors are less than 0.5% for all the schemes. The numerical results also confirm that the proposed technique maintains its excellent performance, even in the face of close to terminal faults with distances down to 4 km, faults with high resistances up to 450 Ω, and noisy signals with signal-to-noise ratios down to 55 dB. Moreover, the comparison results confirm that the proposed approach is more tolerant of measurement noise than the wavelet transform.**

***Index Terms*— Fault location, HVDC transmission, modular multilevel converters, signal segmentation, traveling wave.**

I. Introduction

HALF-BRIDGE modular multilevel converter-based high-voltage direct-current (HBMMC-HVDC) systems are attractive options for bulk power transmission [1] and interconnecting remote sustainable electrical energy sources into the existing power grids [2]. Although HBMMCs cannot limit/control DC-side fault currents [3], they have recently been utilized in commercial projects because of their fundamental advantages in loss, cost, and flexibility [3], [4]. For covering the converter's shortcoming in limiting/controlling fault currents, the world's leading manufacturers have introduced ultrahigh-speed direct-current circuit breakers (DCCBs) [3]. Researchers have also focused on designing suitable ultrahigh-speed fault-detection schemes for HBMMC-HVDC grids [4]. Once a line fault is swiftly detected and isolated, it is vital to accurately estimate its location via a suitable fault-location scheme to perform repair operations as soon as possible. A more accurate fault-location method will result in a shorter outage time and enhance reliability.

Existing fault-location schemes explicitly planned for and assessed in HBMMC-HVDC systems can be divided into three categories:

1) Model-based schemes
2) Artificial intelligence (AI)-based schemes
3) Traveling-wave (TW)-based schemes.

The schemes in the first category have been developed based on simplified models [5], [6]. Although these algorithms have shown good accuracy and performance [5], [6], their essential 5-ms postfault data might be incompatible with the utilization of ultrahigh-speed fault-detection schemes and DCCBs in HBMMC-HVDC grids [7], [8].

The second category comprises the fault-location schemes that have been planned based on AI and pattern-recognition techniques [8], [9]. The input buffered data required in these schemes is compatible with the utilization of ultrahigh-speed relays and DCCBs in HBMMC-HVDC grids [8], [9]. Also, these schemes can provide high generalizability and tolerance dealing with measurement imprecision and noise. However, the need for many appropriately generated learning patterns is one of the most critical challenges in implementing them.

In the third category, researchers have examined the TW theory in different application forms to locate line faults in HBMMC-HVDC systems. In [10], a double-ended TW-based scheme has been presented based on the change of subsequent current samples and tested on a two-terminal system. In [11] and [12], the researchers have applied the continuous wavelet transform on synchronized current samples measured from sensors distributed along lines to extract TW information and estimate the fault location. However, in [12], the estimated locations have also been modified employing the Pearson similarity-based *k*-nearest neighbors algorithm considering 5-

The present work was financially assisted by the Gonbad Kavous University (Project ID: 6-166).

M. Farshad is with the Department of Electrical Engineering, Faculty of Basic Sciences and Engineering, Gonbad Kavous University, Gonbad Kavous 49717-99151, Iran (e-mail: farshad@gonbad.ac.ir).

M. Karimi is with the School of Technology and Innovations, University of Vaasa, Wolffintie 34, FI-65200 Vaasa, Finland (e-mail: mazaher.karimi@uwasa.fi).

ms current data. The authors have shown that the schemes proposed in [11] and [12] are applicable to multiterminal HBMMC-HVDC grids. In addition to the TW-based schemes developed using postfault signals measured before the fault-isolation stage, some methods estimate the location of permanent faults in HBMMC-HVDC grids after the complete isolation of them. For instance, in [13] and [14], the authors have established their schemes on the active signal/pulse injection via faulty lines' hybrid DCCBs and the single-ended identification of subsequent TWs. In [13], the wavelet transform has been applied on single-end current data to identify the reflected TW arrival time at the measuring terminal. However, in [14], the change of subsequent voltage samples has been considered for this purpose. The schemes proposed in [13] and [14] are implementable only if the DCCBs are equipped with controllable solid-state devices.

One of the critical challenges in all the aforesaid TW-based schemes is identifying the incident/reflected TWs. The change of subsequent current and voltage samples considered in [10] and [14] and the wavelet transform coefficients utilized in [11]-[13] can be so sensitive to measurement noise and frequency-dependent reflection factors [15]. This high sensitivity can increase the estimation error and highlight the need for experts to interpret the results. In [15], the researchers have attempted to overcome such a challenge by employing a predictor/corrector technique in a single-ended wavelet transform-based scheme. This technique includes main subroutines: the fault distance and resistance intervals estimation, the reflected TW arrival time calibration, the fault distance formula selection, and the fault distance correction. Despite the acceptable noise tolerance of the method presented in [15], the results have shown that it cannot estimate the location of faults closer than 100 km to the line terminals.

This article seeks to address the abovementioned problems in the TW-based fault-location methods explicitly designed for and evaluated in HBMMC-HVDC systems. In this regard, it proposes a new technique to systematically identify the incident/reflected TWs arrival times at the terminals of HBMMC-HVDC grids without the need for experts. This technique is based on the segmentation of voltage signals captured around the fault-detection instant. Indeed, the captured voltage signals are first scaled and then segmented optimally. Finally, the incident/reflected TWs are easily identified via a simple search algorithm applied to the reconstructed signal segments' differences. Compared to the existing methods, the proposed approach is more tolerant of noise. Also, it can reliably and efficiently detect the incident/reflected TWs in challenging cases, like those generated by faults near the line terminals and high-resistance faults. The proposed technique is applicable in different forms of TW-based fault-location schemes. This article chiefly employs and evaluates this technique in three forms: the single-ended scheme with known TW velocity, the double-ended scheme with known TW velocity, and the double-ended scheme with unknown TW velocity.

The next sections are prepared as follows: Section II provides the TW theory's basic principles, with specific considerations given to HBMMC-HVDC grids. Section III outlines the technique proposed for identifying the incident/reflected TWs arrival times and its application in different TW-based fault-location schemes. Section IV presents and discusses the application results for a test grid. As a final point, Section V concludes.

II. TWs in HBMMC-HVDC Grids

This article focuses on the TW identification in the TW-based fault-location methods explicitly designed for HBMMC-HVDC grids. Hence, the TW theory's basic principles are presented in this section, with specific considerations given to these grids.

After a line fault incident, fault-generated TWs propagate from the fault point towards the line terminals with a polarity opposite to the prefault voltage. These TWs are reflected and refracted many times until complete damping, based on the corresponding coefficients at the line terminals and the fault point. The voltage reflection coefficient at the line terminal, ρ_T, can be calculated as follows [16]:

$$\rho_T = \frac{Z_T - Z_C}{Z_T + Z_C} \tag{1}$$

where Z_T and Z_C are the line's termination and surge impedances, respectively. In HBMMC-HVDC grids, current limiting reactors are usually installed at each line side. They decrease the fault currents' rate-of-rise and keep them below the maximum currents interruptible by the DCCBs and tolerable by the converters until complete fault isolation [17]. Considering this inductive termination element under fault-generated high-frequency transients, ρ_T generally has a magnitude close to one and a small positive phase angle.

The voltage reflection coefficient at the fault point, ρ_F, can also be defined as follows [16]:

$$\rho_F = \frac{-Z_C}{2R_f + Z_C} \tag{2}$$

where R_f is the fault resistance. The refraction coefficient at the fault point equals $1+\rho_F$. As it is clear from (2), ρ_F takes a negative value in the range of (-1,0), depending on R_f.

Fig. 1 shows the lattice diagram [16] for a line fault in a symmetrical monopolar HBMMC-HVDC grid. In this figure, t_0 and t'_0 are the arrival times of the initial incident TWs at the line terminals; t_f and t'_f stand for the arrival times of the first reflected TWs from the fault point; t_r and t'_r signify the arrival times of the first reflected TWs from the remote terminal, and L_{CLR} indicates the inductance of current limiting reactor. It is worth noting that there is no need to know the exact values of reflection and refraction coefficients to locate faults based on the TW theory. However, the range information of these coefficients facilitates identifying the incident/reflected TWs. Considering the abovementioned ranges for the voltage reflection and refraction coefficients, the initial incident TW

This article has been accepted for publication in a future issue of this journal, but has not been fully edited. Content may change prior to final publication. Citation information: DOI 10.1109/TIM.2021.3139688, IEEE Transactions on Instrumentation and Measurement

and the first reflected TW from the remote terminal are of the same polarity. The polarity of the first reflected TW from the fault point is also opposite to them. Moreover, in the case of a resistive fault, the first reflected TW from the fault point arrives at the closest terminal (e.g., terminal *i* in Fig. 1) sooner than other reflected TWs. In contrast, the other terminal (e.g., terminal *j* in Fig. 1) senses the first reflected TW from the remote terminal sooner than other reflected TWs. In the case of solid faults, TWs are not transmitted to another side of the fault point. Fig. 2 demonstrates some positive pole voltage signals measured at terminals *i* and *j* of Fig. 1 for 15-Ω and 0.01-Ω positive-to-negative (p-n) faults simulated at 0.75 s.

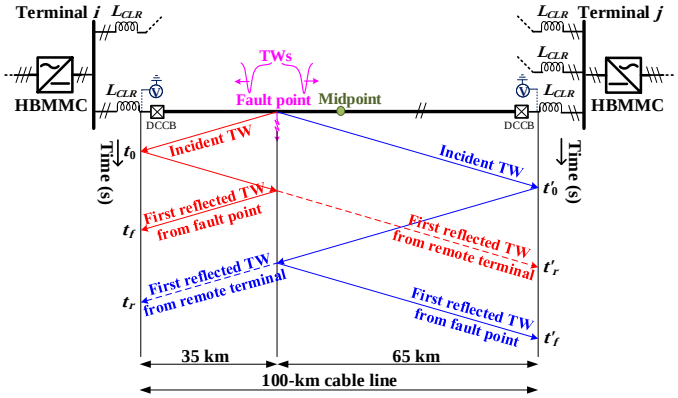

Fig. 1. The lattice diagram for a line fault in a symmetrical monopolar HBMMC-HVDC grid.

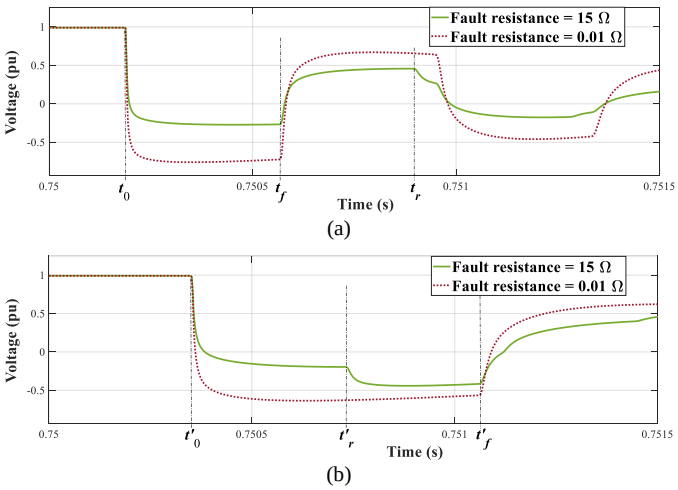

Fig. 2. Positive pole voltage signals for 15-Ω and 0.01-Ω p-n faults simulated at 0.75 s: (a) measured at terminal *i*, (b) measured at terminal *j*.

The postfault behavior of the HBMMCs can be studied in multiple subsequent stages [18]-[20]. However, in this fault-location study, it is enough to consider only the first postfault stage before the ultrafast interruption of fault currents or converter blocking, i.e., the capacitive discharging stage. This stage takes only a few milliseconds. The postfault behavior in this stage is dominantly characterized by discharging the submodule capacitors inserted in each HBMMC arm [20]. In some studies, each HBMMC in the capacitive discharging stage has been modeled as an R-L-C circuit with a natural oscillating response [17], [18], [21]. This natural response is also observable in the voltage signals of Fig. 2 when a TW arrives at the measuring point.

III. TW-Based Fault-Location Schemes

Generally, a real-time fault-detection scheme must work properly and provide correct information for executing an offline fault-location procedure correctly. This article concentrates only on the fault-location problem in HBMMC-HVDC grids. Hence, it is assumed that the ultrahigh-speed fault-detection scheme designated for line protection in HBMMC-HVDC grids can quickly and correctly issue a trip command for line faults. Signal samples buffered around the fault-detection scheme's trip instant are also considered as available input data for fault location.

Accurate identification of TWs arrival times in the measured signals makes it possible to define fault points accurately. The investigation presented in Section II, including the postfault voltage waveform, is used as the foundation to propose a noise-tolerant technique in this section to systematically identify the incident/reflected voltage TWs in HBMMC-HVDC grids without the need for experts. Then, the suggested approach is employed in three forms of TW-based fault-location schemes.

A. Proposed TW Identification Technique

Recognizing the quasi-stepped form of the postfault voltage signals due to the natural response of HBMMCs to TWs in the capacitive discharging stage (e.g., in Fig. 2), a signal segmentation technique is employed for identifying the incident/reflected TWs arrival times.

At first, an input frame comprising the faulty pole's voltage samples buffered around the fault-detection scheme's trip instant, $V^0_{1:n} = [v^0_1, v^0_2, \ldots, v^0_n]$, is considered. This input frame is then scaled as follows:

$$V_{1:n} = \frac{V^0_{1:n} - \min(V^0_{1:n})}{\max(V^0_{1:n}) - \min(V^0_{1:n})} \tag{3}$$

For the given min-max scaled voltage samples, $V_{1:n} = [v_1, v_2, \ldots, v_n]$, the segmentation technique should optimally determine a set of segmentation indices, $S_{1:r} = [s_1, s_2, \ldots, s_r]$. In this segmentation set, each element can take an integer value in the range of 2 to n-1 such that $s_1 < s_2 < \ldots < s_r$. Two dummy indices can also be defined as $s_0 = 1$ and $s_{r+1} = n$.

Several techniques can be used for signal segmentation, among which the techniques based on log-likelihood maximization are ubiquitous [22]. A Gaussian log-likelihood-based technique is also adapted in this article, in which the segmentation indices are obtained by maximizing the following objective function, Γ[23]:

$$\Gamma(s_1, s_2, \ldots, s_r) = -\sum_{a=0}^{r} (s_{a+1} - s_a) \log\left(\sigma^2_{s_a:s_{a+1}-1}\right) \tag{4}$$

where $\sigma^2_{s_a:s_{a+1}-1}$ is the variance of scaled voltage samples with

This article has been accepted for publication in a future issue of this journal, but has not been fully edited. Content may change prior to final publication. Citation information: DOI 10.1109/TIM.2021.3139688, IEEE Transactions on Instrumentation and Measurement

the indices from s_a to $s_{a+1}-1$. This variance is calculated as:

$$\sigma^2_{s_a:s_{a+1}-1} = \frac{1}{s_{a+1}-s_a}\sum_{b=s_a}^{s_{a+1}-1}(v_b - \overline{V_{s_a:s_{a+1}-1}})^2 \quad (5)$$

where $\overline{V_{s_a:s_{a+1}-1}}$ stands for the mean of scaled voltage samples with the indices from s_a to $s_{a+1}-1$.

In this article, the number of segments, r, is considered unknown, i.e., one of the optimization parameters. However, the following constraint is also included in the optimization problem to prevent over-segmentation:

$$s_{a+1} - s_a \geq round(st_{min} \times f_s), \qquad a = 0,1,\dots,r \quad (6)$$

where st_{min} indicates the minimum time length between adjacent segmentation points (i.e., the segment's minimum time length), and f_s is the signal sampling frequency.

The pruned exact linear time (PELT) algorithm [22], [24] provides a suitable procedure for solving the described optimization problem. When the optimal segmentation set is obtained via this solution algorithm, the segmented voltage signal can be reconstructed as:

$$V'_{s_a:s_{a+1}-1} = \overline{V_{s_a:s_{a+1}-1}}, \qquad a = 0,1,\dots,r \quad (7)$$

where $V'_{s_a:s_{a+1}-1}$ is a signal segment that comprises the reconstructed voltage samples with the indices from s_a to $s_{a+1}-1$. The last reconstructed sample, v'_n, can be set equal to v'_{n-1}.

Since the reconstructed signal, $V'_{1:n} = [v'_1, v'_2, \dots, v'_n]$, is noise-free, its TWs arrival instants will be easily identified considering the corresponding voltage sample timestamps, $T_{1:n} = [\tau_1, \tau_2, \dots, \tau_n]$. Here, the following simple search algorithm is designed for this purpose, considering the positive pole's voltage:

1) Calculate differences of adjacent segments as:

$$\Delta sv'_a = v'_{s_a} - v'_{s_{a-1}}, \qquad a = 1,\dots,r \quad (8)$$

2) Find the first element in $\Delta SV'_{1:r} = [\Delta sv'_1, \Delta sv'_2, \dots, \Delta sv'_r]$ that satisfies the following condition:

$$\Delta sv'_p < -\varepsilon_1 \quad (9)$$

where ε_1 takes a small positive value (e.g., 0.015), and p stands for the index of the first found element in $\Delta SV'_{1:r}$. The initial incident TW arrival time is equal to the element with the index of s_p-1 in $T_{1:n}$, i.e., τ_{s_p-1}. It is worth noting that the incident TW results in an abrupt voltage drop due to its opposite polarity relative to the prefault voltage.

3) Find the next element in $\Delta SV'_{1:r}$ that satisfies one of the following conditions:

$$\Delta sv'_q > \varepsilon_1 \quad \& \quad \Delta sv'_q > (1+\varepsilon_2) \times \Delta sv'_{q-1} \quad (10)$$

$$\Delta sv'_q < -\varepsilon_1 \quad \& \quad \Delta sv'_q < (1+\varepsilon_2) \times \Delta sv'_{q-1} \quad (11)$$

where ε_2 also takes a small positive value (e.g., 0.2), and q indicates the index of the next found element in $\Delta SV'_{1:r}$. According to Section II, if this element is found fulfilling (10), it is clear that the identified TW has been reflected from the fault point. If the element is found satisfying (11), it can be comprehended that the identified TW has been reflected from the remote terminal. This TW's arrival time is equal to the element with the index of s_q-1 in $T_{1:n}$, i.e., τ_{s_q-1}.

The above search algorithm will also apply to the negative pole's voltage if the sample values are multiplied by -1 at first. The main steps of the described TW identification technique are represented in Fig. 3 for more clarification.

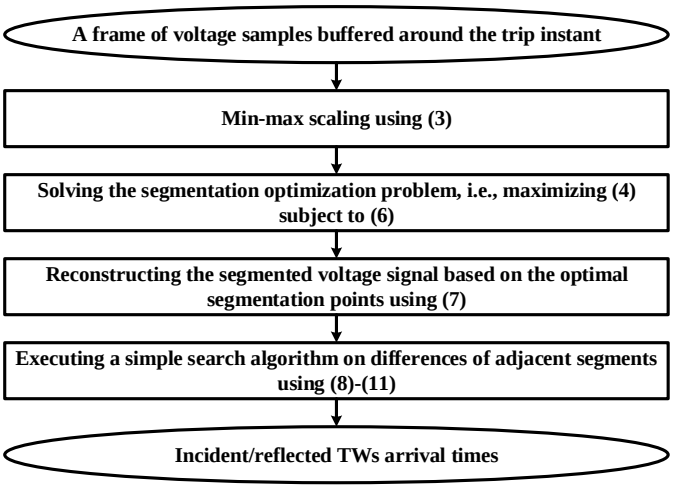

Fig. 3. The main steps of the proposed TW identification technique.

B. Scheme I: Single-Ended Scheme with Known Velocity

The single-ended TW-based scheme estimates the location of fault point based on the time difference of incident and reflected TWs arrival at one of the line terminals, e.g., for terminal i, $\tau^i_{s_q-1} - \tau^i_{s_p-1}$.

If the incident and reflected TWs are identified based on (9) and (10), respectively, then the fault distance is calculated as:

$$x_i = \frac{v_{TW} \times (\tau^i_{s_q-1} - \tau^i_{s_p-1})}{2} \quad (12)$$

where x_i is the fault distance from terminal i, and v_{TW} is the TW velocity.

If the incident and reflected TWs are identified based on (9) and (11), respectively, then the fault distance is estimated as:

$$x_i = L_T - \frac{v_{TW} \times (\tau^i_{s_q-1} - \tau^i_{s_p-1})}{2} \quad (13)$$

where L_T is the line's total length.

In the case of solid faults close to the remote terminal, the single-ended scheme needs the reflected TW from the fault

This article has been accepted for publication in a future issue of this journal, but has not been fully edited. Content may change prior to final publication. Citation information: DOI 10.1109/TIM.2021.3139688, IEEE Transactions on Instrumentation and Measurement

point. Because, in these cases, the reflected TW from the remote terminal is not transmitted towards the measuring end. Hence, for the single-ended scheme, the input frame of voltage samples should include the postfault data with a time length of at least $2L_T/v_{TW}$. Here, the postfault data refers to the captured data after the fault signature arrival at the measuring point.

C. Scheme II: Double-Ended Scheme with Known Velocity

Double-ended TW-based fault-location schemes commonly require synchronized data from both line terminals. The double-ended method with a constant TW velocity estimates the fault distance based on the time difference of incident TWs arrival at the line terminals, e.g., for terminals *i* and *j*, $\tau^{j}_{s_p-1} - \tau^{i}_{s_p-1}$:

$$x_i = \frac{L_T - v_{TW} \times (\tau^{j}_{s_p-1} - \tau^{i}_{s_p-1})}{2} \tag{14}$$

The postfault data length is not discussed in this scheme since the moments of fault signature arrival at the line terminals suffice for fault location.

D. Scheme III: Double-Ended Scheme with Unknown Velocity

If the TW velocity is considered unknown, the double-ended scheme can still estimate the fault location. However, in this case, it also requires the reflected TW arrival time at one of the line terminals. If v_{TW} is derived from (14) in terms of the fault distance and replaced in (12) and (13), the following equations will be formed for the fault distance from terminal *i*:

$$x_i = \frac{L_T \times (\tau^{i}_{s_q-1} - \tau^{i}_{s_p-1})}{2(\tau^{j}_{s_p-1} + \tau^{i}_{s_q-1} - 2\tau^{i}_{s_p-1})} \tag{15}$$

$$x_i = \frac{L_T \times \left(2\tau^{j}_{s_p-1} - \tau^{i}_{s_q-1} - \tau^{i}_{s_p-1}\right)}{2(\tau^{j}_{s_p-1} - \tau^{i}_{s_q-1})} \tag{16}$$

The equation selection follows the same rule expressed for the single-ended scheme in Section III.B. In other words, if the reflected TW's arrival time at terminal *i* (i.e., $\tau^{i}_{s_q-1}$) is obtained based on (10), then (15) should be used, and if it is obtained fulfilling (11), then (16) is valid for fault location. Thanks to the available measurements from both line terminals, similar equations can be rewritten for the fault distance from terminal *j*, i.e., x_j. Also, a similar rule can be adopted to select the appropriate equation. The following averaging equation can then be used to update the estimated fault distance from terminal *i*:

$$x_i \leftarrow \frac{x_i + (L_T - x_j)}{2} \tag{17}$$

The length of required postfault data for this double-ended scheme is the same as for the single-ended method.

E. Input Frame Length

The input frame of samples around the fault-detection scheme's trip instant should generally cover a small part of prefault data, e.g., 0.5 ms of prefault samples. Also, it should cover a minimum length of postfault data, depending on the employed TW-based fault-location scheme. As expressed in Sections III.B and III.D, for schemes I and III, the input frame of voltage samples should include the postfault data with a time length of at least $2L_T/v_{TW}$. As expressed in Section III.C, for scheme II, the postfault data length is not critical since the moments of fault signature arrival at the line terminals suffice for fault location. Then, for this scheme, the input frame should cover only a small part of postfault data, e.g., 0.5 ms of postfault samples. It is noteworthy that it is acceptable to consider a wider input frame to ensure meeting the abovementioned conditions.

IV. Results and Discussions

A ±320 kV symmetrical monopolar HBMMC-HVDC grid [25] is simulated using the PSCAD/EMTDC software package [26] under different fault conditions expressed in the following subsections. The single-line diagram of this test grid is depicted in Fig. 4. Some essential specifications are also given in Table I. The voltage signals acquired from this simulated system are then stored and imported to the MATLAB environment [27]. The proposed technique is also programmed in the MATLAB environment and applied to the imported signals for fault location based on the three schemes described in Section III. The diagram for this procedure is depicted in Fig. 5. In this implementation, the segment's minimum time length, st_{min}, is set to 40 μs. It is worth noting that in the fault-location studies, the error is calculated as follows [28]:

$$e = \frac{|d_i - x_i|}{L_T} \times 100 \tag{18}$$

where *e* is the percentage estimation error, and d_i is the actual fault distance from terminal *i*.

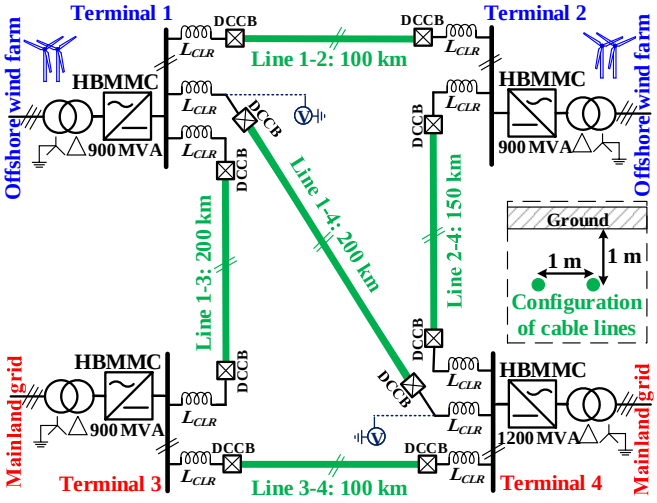

Fig. 4. The simulated HBMMC-HVDC grid.

This article has been accepted for publication in a future issue of this journal, but has not been fully edited. Content may change prior to final publication. Citation information: DOI 10.1109/TIM.2021.3139688, IEEE Transactions on Instrumentation and Measurement

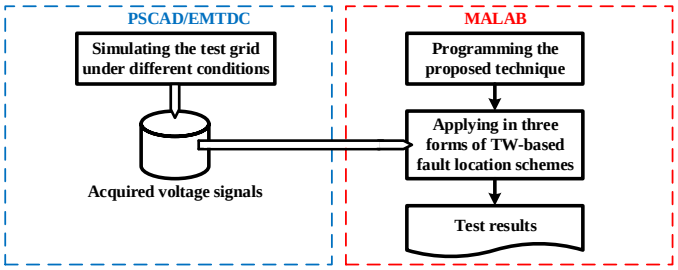

Fig. 5. The diagram of the test procedure.

TABLE I
SOME SPECIFICATIONS OF THE SIMULATED TEST GRID

Model of converters	Continuous [29]
Internal control scheme of converters	Stored energy estimation [30]
Type of cables	320 kV XLPE-insulated [25]
Model of cables	Frequency-dependent (phase) [26]
v_{TW} in simulated cables	183500 km/s [25]
L_{CLR} for current limiting reactors	150 mH
f_s for signal sampling	250 kHz

A. TW Identification Performance

Fig. 6 demonstrates the segmentation and TW identification performance of the proposed technique for the positive pole voltage signals captured at terminal 1 for some positive-to-ground (p-g) faults in line 1-4 at 0.78 s, considering different fault distances from terminal 1 and fault resistances, i.e., d_1 and R_f. As comprehendible from this figure, the proposed technique can accurately identify the incident/reflected TWs arrival times.

Some p-g and p-n faults are also simulated in line 1-4, considering various fault locations and resistances. The suggested TW identification technique is applied to the captured voltage signals for fault location based on the three TW-based fault-location plans described in Section III. The fault-location results for the p-g and p-n faults are given in Tables II and III, respectively. According to these tables, scheme I (i.e., single-ended scheme with known TW velocity) has estimated the fault locations well except for the very close faults with a distance less than 4 km to one of the line terminals. For this scheme, the errors related to the faults at distances of 2 km from the terminals (i.e., d_1=2 km and d_1=198 km) have exceeded 2%. It is noteworthy that a close to terminal fault can make it more difficult to distinguish the reflected TW because of its short time interval relative to the incident TW. In contrast, scheme II (i.e., double-ended scheme with known TW velocity) has performed more accurately. For this scheme, considering all the fault distances from 2 km to 198 km from terminal 1, the errors have not exceeded 0.1%. Also, the errors have not changed for the changes in fault resistance. Indeed, the results related to scheme II are pretty independent of fault location and resistance since it requires identifying only the incident TWs. These TWs are easier to identify because of the sharp voltage drop at their arrival moments. Scheme III (i.e., double-ended scheme with unknown TW velocity) has shown an accuracy better than scheme I and lower than scheme II. Similar to scheme I, this scheme is also not very accurate for the faults at 2 km and 198 km due to the need to identify the reflected TWs. The average fault-location errors are less than 0.5% for all the schemes. These results confirm that the proposed technique has an acceptable TW identification ability and is employable in different TW-based plans.

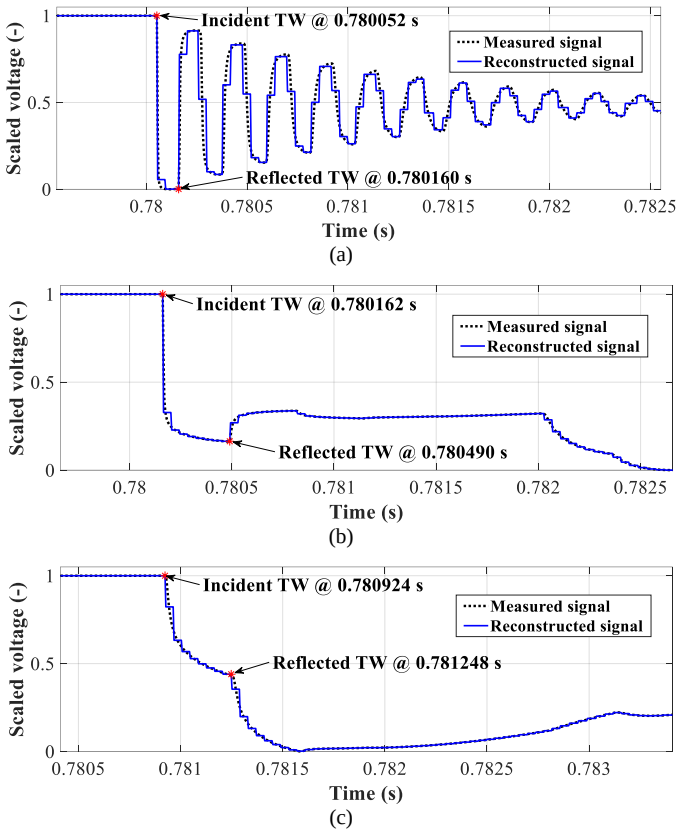

Fig. 6. The segmentation and identification performance for the positive pole voltage signals captured at terminal 1 for p-g faults in line 1-4 at 0.78 s: (a) d_1=10 km & R_f=0.01 Ω, (b) d_1=30 km & R_f=50 Ω, (c) d_1=170 km & R_f=100 Ω.

TABLE II
PERCENTAGE ESTIMATION ERRORS FOR P-G FAULTS IN LINE 1-4

	e (%) for scheme I			e (%) for scheme II			e (%) for scheme III		
$d_1 \downarrow$ $R_f \rightarrow$	0.01 Ω	50 Ω	100 Ω	0.01 Ω	50 Ω	100 Ω	0.01 Ω	50 Ω	100 Ω
2 km	2.12	1.20	0.82	0.09	0.09	0.09	1.57	0.97	0.71
4 km	0.02	0.20	0.20	0.01	0.01	0.01	0.07	0.28	0.11
10 km	0.05	0.60	0.60	0.05	0.05	0.05	0.12	0.05	0.05
30 km	0.14	0.05	0.05	0.04	0.04	0.04	0.30	0.11	0.02
60 km	0.09	0.09	0.09	0.00	0.00	0.00	0.04	0.07	0.00
140 km	0.09	0.46	0.28	0.00	0.00	0.00	0.04	0.07	0.04
170 km	0.88	0.23	0.14	0.04	0.04	0.04	0.30	0.11	0.02
190 km	0.42	0.51	0.51	0.05	0.05	0.05	0.12	0.05	0.05
196 km	0.17	0.39	0.20	0.01	0.01	0.01	0.07	0.28	0.19
198 km	1.92	0.83	0.83	0.09	0.09	0.09	1.82	0.97	0.63
Average	**0.47**			**0.04**			**0.31**		

TABLE III
PERCENTAGE ESTIMATION ERRORS FOR P-N FAULTS IN LINE 1-4

	e (%) for scheme I			e (%) for scheme II			e (%) for scheme III		
$d_1 \downarrow$ $R_f \rightarrow$	0.01 Ω	50 Ω	100 Ω	0.01 Ω	50 Ω	100 Ω	0.01 Ω	50 Ω	100 Ω
2 km	2.12	1.02	1.20	0.09	0.09	0.09	1.82	0.97	0.97
4 km	0.02	0.20	0.20	0.01	0.01	0.01	0.07	0.28	0.02
10 km	0.05	0.41	0.60	0.05	0.05	0.05	0.52	0.03	0.05
30 km	0.14	0.14	0.05	0.04	0.04	0.04	0.42	0.05	0.11
60 km	0.09	0.09	0.09	0.00	0.00	0.00	0.00	0.00	0.04
140 km	0.09	0.46	0.09	0.00	0.00	0.00	0.00	0.11	0.00
170 km	1.43	0.23	0.23	0.04	0.04	0.04	0.48	0.05	0.11
190 km	0.42	0.51	0.51	0.05	0.05	0.05	0.12	0.03	0.05
196 km	0.17	0.17	0.17	0.01	0.01	0.01	0.07	0.02	0.02
198 km	1.92	0.83	0.83	0.09	0.09	0.09	1.82	0.89	0.97
Average	**0.48**			**0.04**			**0.34**		

This article has been accepted for publication in a future issue of this journal, but has not been fully edited. Content may change prior to final publication. Citation information: DOI 10.1109/TIM.2021.3139688, IEEE Transactions on Instrumentation and Measurement

B. Performance with Lower Sampling Frequencies

Based on the analysis performed in [31], even in an ideal condition with the correct identification of the samples related to the TWs arrival, the fault location estimation may encounter an error due to signal sampling and the discrete sample times. According to Table I, the set sampling frequency is 250 kHz. Here, additional tests are performed with the same conditions of Tables II and III but with lower sampling frequencies. The average errors for different sampling frequencies are compared in Table IV. As expected, the TW-based schemes' accuracy has reduced with lowering the sampling frequency. However, this accuracy reduction is more significant for scheme I and less noticeable for scheme II. It is worth pointing out that scheme I encounters a combination of errors due to signal sampling and the reflected TW identification difficulties for close to terminal and high-resistance faults. This combination has manifested itself as a more severe reduction in the accuracy at the lower sampling frequencies. In contrast, it seems that scheme II does not face such an error combination since it requires identifying only the incident TWs, which are less challenging due to the sharp voltage change at their arrival moments.

TABLE IV
AVERAGE ERRORS FOR DIFFERENT SAMPLING FREQUENCIES

	e (%) for scheme I		*e* (%) for scheme II		*e* (%) for scheme III	
$f_s \downarrow$	p-g faults	p-n faults	p-g faults	p-n faults	p-g faults	p-n faults
250 kHz	0.47	0.48	0.04	0.04	0.31	0.34
125 kHz	0.76	0.73	0.11	0.11	0.67	0.64
62.5 kHz	1.09	1.23	0.19	0.19	0.87	1.09

C. Noise Effects

For more investigations, the suggested TW identification technique is applied to noisy signals for fault location based on schemes I, II, and III. The fault-location results for different p-g faults in line 1-4 considering a signal-to-noise ratio (SNR) of 55 dB are given in Table V. There are no remarkable differences in the results of this table compared to the ones presented in Table II. In other words, the proposed technique has a high tolerance to the applied level of random noise. However, it is clear that if the measurement noise level increases (i.e., SNR decreases) significantly, the TW identification will be so challenging, especially for the reflected TW in the case of close to terminal and high-resistance faults.

TABLE V
PERCENTAGE ESTIMATION ERRORS FOR P-G FAULTS IN LINE 1-4 (SNR=55 DB)

	e (%) for scheme I			*e* (%) for scheme II			*e* (%) for scheme III		
$d_1 \downarrow$ $R_f \rightarrow$	0.01 Ω	50 Ω	100 Ω	0.01 Ω	50 Ω	100 Ω	0.01 Ω	50 Ω	100 Ω
2 km	2.12	1.20	0.46	0.09	0.27	0.27	1.65	0.97	0.35
4 km	0.02	0.20	0.20	0.17	0.17	0.17	0.27	0.10	0.10
10 km	0.05	0.78	0.14	0.05	0.23	0.23	0.67	0.15	0.26
30 km	0.14	0.05	0.23	0.14	0.14	0.14	0.05	0.05	0.12
60 km	0.09	0.28	0.83	0.00	0.00	0.00	0.18	0.07	0.18
140 km	0.65	0.09	0.09	0.00	0.00	0.00	0.11	0.07	0.22
170 km	1.24	0.23	0.23	0.14	0.14	0.14	0.24	0.05	0.05
190 km	0.42	0.51	0.51	0.05	0.23	0.23	0.13	0.26	0.42
196 km	0.17	0.02	0.02	0.01	0.17	0.17	0.07	0.10	0.10
198 km	1.92	0.83	0.83	0.09	0.27	0.27	1.82	0.97	0.26
Average	**0.48**			**0.13**			**0.34**		

D. High-Resistance Faults

Some p-g faults are also simulated at different places of line 1-4, considering higher fault resistances of 250 Ω, 350 Ω, and 450 Ω. The suggested TW identification technique is then applied to the captured voltage signals for fault location based on schemes I, II, and III. The relevant results are given in Table VI. Based on this table, all the schemes have shown relatively accurate performance for high-resistance faults thanks to the excellent identification ability of the proposed technique. However, comparing these results with the ones presented in Table II, especially in the case of faults not very close to the terminals, the higher fault resistances have degraded the accuracy of schemes I and III to some extent. A higher fault resistance can make it more difficult to identify the reflected TW due to lower reflection and higher refraction at the fault point. In contrast, scheme II has remained utterly immune to the adverse effects of high-resistance faults since it requires identifying only the incident TWs.

TABLE VI
PERCENTAGE ESTIMATION ERRORS FOR HIGH-RESISTANCE P-G FAULTS IN LINE 1-4

	e (%) for scheme I			*e* (%) for scheme II			*e* (%) for scheme III		
$d_1 \downarrow$ $R_f \rightarrow$	250 Ω	350 Ω	450 Ω	250 Ω	350 Ω	450 Ω	250 Ω	350 Ω	450 Ω
2 km	0.82	0.82	0.82	0.09	0.09	0.09	0.71	0.71	0.71
4 km	0.72	0.72	0.72	0.01	0.01	0.01	0.63	0.63	0.63
10 km	0.32	0.60	0.60	0.05	0.05	0.05	0.36	0.44	0.44
30 km	0.23	0.51	0.51	0.04	0.04	0.04	0.17	0.30	0.30
60 km	0.28	0.28	0.28	0.00	0.00	0.00	0.11	0.04	0.04
140 km	0.28	0.09	0.09	0.00	0.00	0.00	0.11	0.07	0.07
170 km	0.23	0.23	0.23	0.04	0.04	0.04	0.17	0.30	0.30
190 km	0.51	0.51	0.51	0.05	0.05	0.05	0.36	0.53	0.44
196 km	0.57	0.57	0.17	0.01	0.01	0.01	0.37	1.21	0.86
198 km	0.83	0.83	0.83	0.09	0.09	0.09	0.71	0.71	0.71
Average	**0.49**			**0.04**			**0.44**		

E. Comparison

Here, the proposed TW identification technique is compared to other strategies utilized so far in the TW-based fault-location methods explicitly designed for and assessed in HBMMC-HVDC systems.

Using the change of subsequent samples for TW identification is computationally efficient and straightforward [10], [14]. However, it does not seem a good idea in the case of noisy measurements since such a simple form of numerical differentiation will inherently amplify high-frequency noise [32]. Since the fault-location procedure is usually executed offline, it is possible to employ more complicated signal processing tools. The wavelet transform is one of the most widely used tools for identifying the incident/reflected TWs [11]-[13]. Here, a p-n fault is simulated in line 1-4 at 0.78s, considering d_1=60 km and R_f=100 Ω. The continuous wavelet transform considering the Haar wavelet at the scales from 1 to 128 [27] and the proposed technique are then applied to the positive pole voltage signals captured at terminal 1 with different SNRs. Fig. 7 presents the obtained wavelet transform local maxima lines for these noise-free and noisy signals. Also, Fig. 8 exhibits the segmentation and TW identification performance of the proposed approach.

This article has been accepted for publication in a future issue of this journal, but has not been fully edited. Content may change prior to final publication. Citation information: DOI 10.1109/TIM.2021.3139688, IEEE Transactions on Instrumentation and Measurement

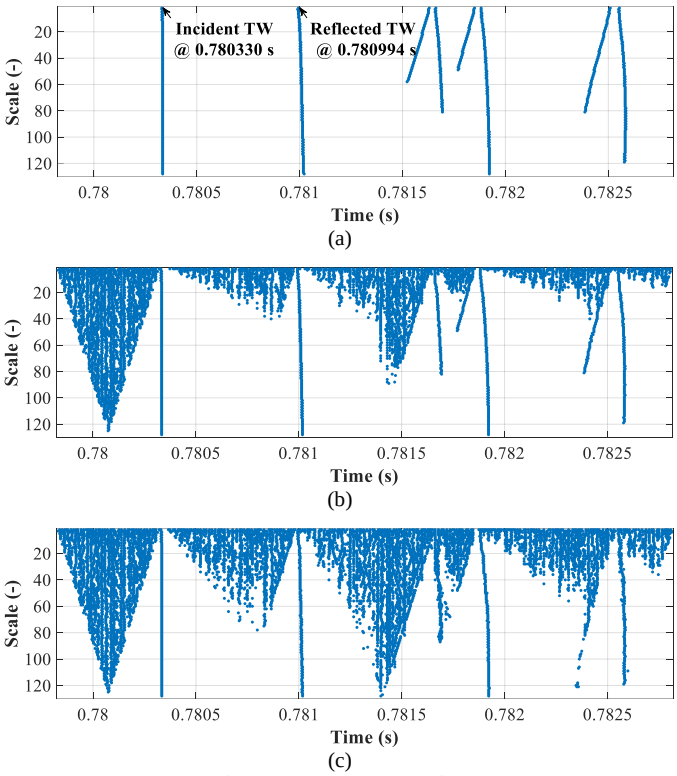

Fig. 7. The wavelet transform local maxima lines for the positive pole voltage signals captured at terminal 1 for a p-n fault in line 1-4 at 0.78 s, considering d_1=60 km and R_f=100 Ω: (a) SNR=∞ , (b) SNR= 70 dB, (c) SNR=55 dB.

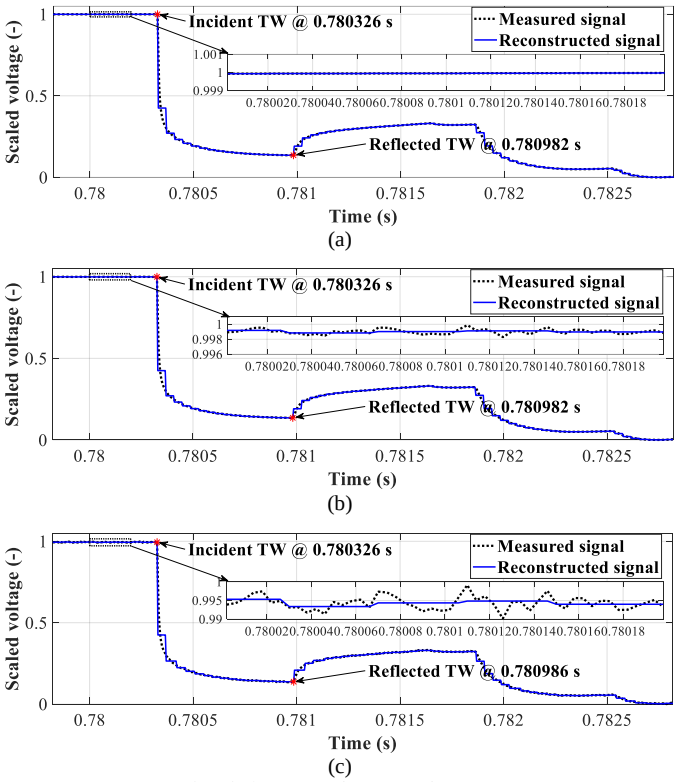

Fig. 8. The proposed technique's performance for the positive pole voltage signals captured at terminal 1 for a p-n fault in line 1-4 at 0.78 s, considering d_1=60 km and R_f=100 Ω: (a) SNR=∞ , (b) SNR= 70 dB, (c) SNR=55 dB.

Based on Figs. 7(a) and 8(a), when the signals are not noisy (i.e., SNR=∞), both methods have suitable output results that can be used to routinely identify the incident/reflected TWs arrival times. In other words, without the need for experts to interpret the results, a simple routine is programmable to easily extract the incident/reflected TWs arrival times from their output results. According to Figs. 7(b) and 7(c), in the noisy cases where the SNR is reduced to 70 and 55 dB, the output results of the wavelet transform include the false local maxima lines due to the random measurement noise, which makes it very difficult to identify the incident/reflected TWs routinely. Hence, at least there is a need for experts to review and interpret these output results. In contrast, according to Figs. 8(b) and 8(c) and the results of Table V, the proposed technique can easily identify the incident/reflected TWs arrival times under such reasonable noise levels by executing the designed algorithm and routine presented in Section III.A.

In [15], the researchers have attempted to eliminate the false wavelet transform modulus maxima (WTMM) points resulting from high-frequency noise by employing a predictor/corrector technique in a single-ended fault-location scheme. However, the method presented in [15] has failed to estimate the location of faults closer than 100 km to the line terminals. In contrast, according to the results of Tables II, III, and V, the single-ended fault-location scheme with the proposed technique has accurately estimated the location of very close faults with distances down to 4 km to the line terminals.

V. Conclusion

This article proposed an innovative technique for determining the incident/reflected TWs arrival times in HBMMC-HVDC grids methodically based on voltage signal segmentation. This technique can be adapted to and employed in different TW-based fault-location plans. This article described how to use the proposed technique in three common forms of TW-based fault-location schemes. Fault location in a test grid employing this technique was associated with an average error of less than 0.5% in all the TW-based fault-location schemes. The presented approach could acceptably perform even for the faults near the line terminals and at sampling frequencies of less than 100 kHz, sacrificing a degree of accuracy. The proposed technique performed excellently in the case of noisy signals with an SNR of 55 dB and high fault resistances up to at least 450 Ω. The proposed technique could better deal with measurement noise than the wavelet transform in a comparative study. Despite all the performed tests and comparisons, verifying the proposed technique's performance with the experimental data should be considered in future studies.

References

[1] L. I. U. C, F. Zhuo, and F. Wang, "Fault diagnosis of commutation failure using wavelet transform and wavelet neutral network in HVDC

transmission system," *IEEE Trans. Instrum. Meas.*, vol. 70, Art. seq. no. 3525408, 2021.

[2] R. Ferdinand, M. Cupelli, and A. Monti, "Multipoint synchronized recordings in offshore wind farms with continuous measurement power quality meters," *IEEE Trans. Instrum. Meas.*, vol. 67, no. 12, pp. 2785-2795, Dec. 2018.

[3] S. Du, A. Dekka, B. Wu, and N. Zargari, *Modular Multilevel Converters: Analysis, Control, and Applications*. Hoboken, NJ, USA: Wiley-IEEE Press, 2018.

[4] N. Tong, X. Lin, Y. Li, Z. Hu, N. Jin, F. Wei, and Z. Li, "Local measurement-based ultra-high-speed main protection for long distance VSC-MTDC," *IEEE Trans. Power Deliv.*, vol. 34, no. 1, pp. 353-364, Feb. 2019.

[5] J. Xu, L. Y, C. Zhao, and J. Liang, "A model based dc fault location scheme for multi-terminal MMC-HVDC systems using a simplified transmission line representation," *IEEE Trans. Power Deliv.*, vol. 35, no. 1, pp. 386-395, Feb. 2020.

[6] B. Wang, Y. Liu, D. Lu, K. Yue, and R. Fan, "Transmission line fault location in MMC-HVDC grids based on dynamic state estimation and gradient descent," *IEEE Trans. Power Deliv.*, vol. 36, no. 3, pp. 1714-1725, Jun. 2021.

[7] Y. Song, J. Sun, M. Saeedifard, S. Ji, L. Zhu, and A. P. S. Meliopoulos, "Optimum selection of circuit breaker parameters based on analytical calculation of overcurrent and overvoltage in multiterminal HVDC grids," *IEEE Trans. Ind. Electron.*, vol. 67, no. 5, pp. 4133-4143, May 2020.

[8] M. Farshad, "Fault location in HVDC grids equipped with quick-action protections and circuit breakers based on voltage transient response," *IEEE Trans. Ind. Electron.*, vol. 68, no. 12, pp. 12881-12889, Dec. 2021.

[9] D. Tzelepis, S. Mirsaeidi, A. Dysko, Q. Hong, J. He, and C. D. Booth, "Intelligent fault location in MTDC networks by recognising patterns in hybrid circuit breaker currents during fault clearance process," *IEEE Trans. Industr. Inform.*, vol. 17, no. 5, pp. 3056-3068, May 2021.

[10] X. Zheng, M. H. Nadeem, N. Tai, S. Habib, B. Wang, M. Yu, and Y. He, "A transient current protection and fault location scheme for MMC-HVDC transmission network," *Int. J. Electr. Power Energy Syst.*, vol. 124, Art. no. 106348, Jan. 2021.

[11] D. Tzelepis, G. Fusiek, A. Dyśko, P. Niewczas, C. Booth, and X. Dong, "Novel fault location in MTDC grids with non-homogeneous transmission lines utilizing distributed current sensing technology," *IEEE Trans. Smart Grid*, vol. 9, no. 5, pp. 5432-5443, Sep. 2018.

[12] D. Tzelepis, A. Dyśko, G. Fusiek, P. Niewczas, S. Mirsaeidi, C. Booth, and X. Dong, "Advanced fault location in MTDC networks utilising optically-multiplexed current measurements and machine learning approach," *Int. J. Electr. Power Energy Syst.*, vol. 97, pp. 319-333, Apr. 2018.

[13] S. Zhang, G. Zou, B. Li, B. Xu, and J. Li, "Fault property identification method and application for MTDC grids with hybrid dc circuit breaker," *Int. J. Electr. Power Energy Syst.*, vol. 110, pp. 136-143, Sep. 2019.

[14] G. Song, T. Wang, and K. S. T. Hussain, "DC line fault identification based on pulse injection from hybrid HVDC breaker," *IEEE Trans. Power Deliv.*, vol. 34, no. 1, pp. 271-280, Feb. 2019.

[15] C. Zhang, G. Song, T. Wang, and L. Yang, "Single-ended traveling wave fault location method in dc transmission line based on wave front information," *IEEE Trans. Power Deliv.*, vol. 34, no. 5, pp. 2028-2038, Oct. 2019.

[16] L. V. Bewley, "Traveling waves on transmission systems," *Trans. Am. Inst. Elect. Eng.*, vol. 50, no. 2, pp. 532-550, Jun. 1931.

[17] Y. Wang, W. Wen, C. Zhang, Z. Chen, and C. Wang, "Reactor sizing criterion for the continuous operation of meshed HB-MMC-based MTDC system under dc faults," *IEEE Trans. Ind. Appl.*, vol. 54, no. 5, pp. 5408-5416, Sep.-Oct. 2018.

[18] W. Leterme, J. Beerten, and D. V. Hertem, "Equivalent circuit for half-bridge MMC dc fault current contribution," in *IEEE Int. Energy Conf. (ENERGYCON)*, Leuven, Belgium, 2016, pp. 1-6.

[19] O. Cwikowski, A. Wood, A. Miller, M. Barnes, and R. Shuttleworth, "Operating dc circuit breakers with MMC," *IEEE Trans. Power Deliv.*, vol. 33, no. 1, pp. 260-270, Feb. 2018.

[20] J. Qin, M. Saeedifard, A. Rockhill, and R. Zhou, "Hybrid design of modular multilevel converters for HVDC systems based on various submodule circuits," *IEEE Trans. Power Deliv.*, vol. 30, no. 1, pp. 385-394, Feb. 2015.

[21] W. Leterme, J. Beerten, and D. V. Hertem, "Nonunit protection of HVDC grids with inductive dc cable termination," *IEEE Trans. Power Deliv.*, vol. 31, no. 2, pp. 820-828, Apr. 2016.

[22] C. Truong, L. Oudre, and N. Vayatis, "Selective review of offline change point detection methods," *Signal Process.*, vol. 167, p. 107299, Feb. 2020.

[23] M. Lavielle, "Using penalized contrasts for the change-point problem," *Signal Process.*, vol. 85, no. 8, pp. 1501-1510, Aug. 2005.

[24] R. Killick, P. Fearnhead, and I. A. Eckley, "Optimal detection of changepoints with a linear computational cost," *J. Am. Stat. Assoc.*, vol. 107, no. 500, pp. 1590-1598, Dec. 2012.

[25] W. Leterme, N. Ahmed, J. Beerten, L. Ängquist, D. V. Hertem, and S. Norrga, "A new HVDC grid test system for HVDC grid dynamics and protection studies in EMT-type software," in *11th IET Int. Conf. AC DC Power Transm.*, Birmingham, UK, 2015, pp. 1-7.

[26] *PSCAD User's Guide*, Manitoba HVDC Research Ctr., Winnipeg, MB, Canada, 2018.

[27] *MATLAB User's Guide: R2020b Documentation*, MathWorks Inc, Natick, MA, USA, 2020.

[28] S. Lin, L. Liu, P. Sun, Y. Lei, Y. Teng, and X. Li, "Fault location algorithm based on characteristic- harmonic measured impedance for HVdc grounding electrode lines," *IEEE Trans. Instrum. Meas.*, vol. 69, no. 12, pp. 9578-9585, Dec. 2020.

[29] N. Ahmed, L. Ängquist, S. Norrga, A. Antonopoulos, L. Harnefors, and H. Nee, "A computationally efficient continuous model for the modular multilevel converter," *IEEE J. Emerg. Sel. Topics Power Electron.*, vol. 2, no. 4, pp. 1139-1148, Dec. 2014.

[30] L. Angquist, A. Antonopoulos, D. Siemaszko, K. Ilves, M. Vasiladiotis, and H. Nee, "Open-loop control of modular multilevel converters using estimation of stored energy," *IEEE Trans. Ind. Appl.*, vol. 47, no. 6, pp. 2516-2524, Nov.-Dec. 2011.

[31] F. B. Costa, F. V. Lopes, K. M. Silva, K. M. C. Dantas, R. L. S. França, M. M. Leal, and R. L. A. Ribeiro, "Mathematical development of the sampling frequency effects for improving the two-terminal traveling wave-based fault location," *Int. J. Electr. Power Energy Syst.*, vol. 115, Art. no. 105502, Feb. 2020.

[32] B. Carlsson, A. Ahlen, and M. Sternad, "Optimal differentiation based on stochastic signal models," *IEEE Trans. Signal Process.*, vol. 39, no. 2, pp. 341-353, Feb. 1991.

Mohammad Farshad was born in Gonbad Kavous, Iran, in 1981. He received the B.Sc. degree in power transmission and distribution networks engineering from the Power and Water University of Technology (PWUT), Tehran, Iran, in 2003, and the M.Sc. and Ph.D. degrees in power system engineering from the Ferdowsi University of Mashhad, Mashhad, Iran, in 2006 and 2013, respectively.

He is currently an Assistant Professor with the Department of Electrical Engineering, Faculty of Basic Sciences and Engineering, Gonbad Kavous University. His main research interest includes the application of soft computing techniques in power system protection, operation, and planning.

Mazaher Karimi (M'11) received his Ph.D. degree in Electrical Energy and Power System from the University of Malaya, Kuala Lumpur, Malaysia, in 2013. He worked as a Research Associate with The University of Manchester, from 2016 to 2017. From 2017 to 2020, he was an Assistant Professor at Gonbad Kavous University, Iran.

Currently, he is an Assistant Professor with the School of Technology and Innovations, University of Vaasa, Vaasa, Finland. His current research interests include smart grid applications; wide-area monitoring, protection, and control; distributed generation; power system stability and frequency control.